Proceedings of the ASME 2022 17th International Manufacturing Science and Engineering Conference
MSEC2022
June 27-July 1, 2022, West Lafayette, Indiana, USA

MSEC2022-85950

USING AN ARTICULATED INDUSTRIAL ROBOT TO PERFORM CONFORMAL DEPOSITION WITH MESOSCALE FEATURES

Ying Cai, Prahar M. Bhatt, Hangbo Zhao, and Satyandra K. Gupta *
Center for Advanced Manufacturing, University of Southern California, Los Angeles, California 90007
Email: [yingcai,praharbh,hangbozh,guptask]@usc.edu

ABSTRACT

Six Degrees of Freedom (DOF) robotic manipulators can use non-planar layers to deposit materials in additive manufacturing. Conformal material deposition requires accurately positioning and orienting the deposition tool on non-planar surfaces. Using industrial manipulators to move the deposition tool enables 6 DOF motion and avoids collision between the tool and the pre-existing substrate. Regular articulated industrial robots have high repeatability but do not exhibit high accuracy. Therefore, performing printing that involves small features becomes challenging. In this paper, we present advances in non-planar surface registration with respect to the robot frame, deposition tool calibration, and gap compensation scheme to enable accurate positioning of the tool tip with respect to the non-planar substrate. This enables us to maintain an accurately controlled gap between the tool tip and the underlying surface to allow printing of mesoscale features on curved surfaces. We test the efficacy of the proposed approach by printing a single layer of ink patterns with approximately 130 µm line width on spherical (radius $<$ 1 cm), cylindrical, and planar substrates. We also demonstrate the capability of changing tool orientation enabled by the 6 DOF robotic manipulator and show that adjusting tool orientation is critical in enabling conformal printing on highly curved surfaces. Finally, the gap variation is characterized and accurate control of the gap is demonstrated.

Keywords: robotic manipulator, conformal printing, mesoscale printing, workpiece registration, TCP estimation, gap compensation.

1 Introduction

Material deposition is a fundamental capability behind many of the popular additive manufacturing processes [1]. In conventional additive manufacturing, material deposition is performed on planar horizontal surfaces. Creating a conformal geometry requires stacking multiple planar layers to approximate the desired geometry. This restricts the types of devices that can be realized and also limits their performance due to poor shape approximation and inferior mechanical properties at layer interfaces. There are various applications where conformal deposition with mesoscale features is expected to be useful. Examples include printing of interconnects for flexible electronics, wearable devices, microfluidic devices, robotic skins, and sensors (Figure 1) [2–7]. Conformal deposition enables direct printing on three-dimensional (3D) surfaces without requiring planar approximation [8]. Conformal printing capability also enables printing over prefabricated components that have been inserted during the printing process [9].

In principle, conformal deposition can be performed using a 3 DOF gantry-based system. This approach enables accurate positioning of deposition tools. However, tool orientation cannot be changed by a 3 DOF positioning system. Material deposition on complex surfaces may require tool orientation to be changed based on the local direction normal and curvature to make sure that material is transferred from the deposition tool to the surfaces at the desired rate and pressure. When the surface is geometrically complex, avoiding tool and surface collision may also require tool orientation to be changed [10, 11]. These requirements mean that we need to consider a 6 DOF motion for the deposition tool so that both its position and orientation can be

*Address all correspondence to this author.

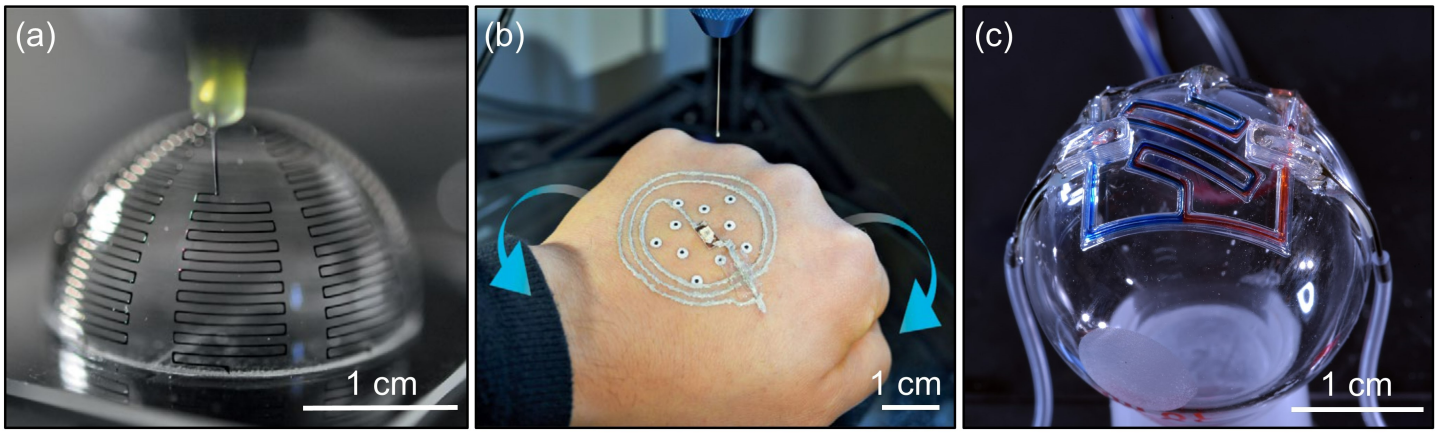

FIGURE 1: Conformal 3D printing on non-planar surfaces: (a) 3D printed antenna on a hemispherical surface [5]; (b) 3D printed inductive coil on a human hand [6]; (c) 3D printed microfluidic channels on a spherical surface [7].

controlled.

Robotic manipulators can be used to control the position and orientation of deposition tools during conformal material deposition and avoid collision between the tool and the pre-existing substrate [12]. Conformal deposition requires accurately positioning the deposition tool on non-planar surfaces. Traditional articulated industrial robots have high repeatability but do not exhibit high accuracy due to execution errors [13, 14]. Therefore, performing material deposition that involves features with small size becomes very challenging.

Successful material deposition requires maintaining an appropriate gap between the tool tip and the surface. Excessive gap may lead to poor material placement accuracy. On the other hand, if the gap is too small, the material cannot be extruded out of the tool, which may clog the tool. In this paper, we present advances in non-planar surface registration with respect to the robot frame, robot calibration, deposition tool calibration, and gap compensation scheme to enable accurate positioning of the tool tip with respect to non-planar substrates. This enables us to maintain an appropriate gap between the tool tip and the underlying surface and enables the printing of small features. We test the efficacy of the proposed approach by printing several different types of patterns with small line width on spherical, cylindrical, and planar substrates. We also demonstrate the capability and advantages of using the 6 DOF robotic manipulator to adjust the tool orientation for printing mesoscale features on highly curved surfaces, as compared to printing with constant tool orientation. Finally, we characterize the gap variation to evaluate the proposed approach.

2 Related Work

Material extrusion-based mesoscale conformal printing has primarily relied on three-axis gantry motion systems on which deposition tools (e.g., nozzles) are mounted. Cohen *et al.* reported one of the early works in this area in which they utilized a three-axis motion system to deposit hydrogels on the femur for the in-situ repair of osteochondral defects with relatively large line widths (approximately 0.8 mm) [15]. Using a similar motion system with microscale nozzles (100 μm and 30 μm diameters), Adam *et al.* fabricated 3D antennas by direct ink writing of conductive epoxy on convex and concave surfaces of a glass hemisphere [5]. Silver serpentine patterns with a line width as small as 150-200 μm were printed on the hemisphere, which contributes to improved antenna bandwidth over planar designs. One significant limitation of their system is that the nozzle needs to be manually bent at an angle to facilitate printing for small nozzles due to the incapability of adjusting the nozzle orientation with respect to curved surfaces. Other works using three-axis gantry motion systems include the fabrication of polymer photodetectors [16] and wireless ion sensors [17] printed on hemispherical surfaces, with typical line widths in the range of hundreds of microns.

More recently, low DOF robotic systems such as delta robots have been used for conformal mesoscale printing. Zhu *et al.* used an adaptive 3D printing platform consisting of a delta robot, monitor cameras, and tracking cameras for localization of the target surface. They demonstrated the printing of functional and biological materials on moving freeform surfaces such as human hands and the mouse [6]. A closed-loop feedback system enables the corrections of printing errors introduced by the movement of freeform surfaces. The same research group also demonstrated 3D printed self-supporting elastomeric microfluidic structures on spherical glass [7].

Finally, research has been done on using 6 DOF articulated industrial manipulators to perform millimeter-scale conformal 3D printing [18]. Bhatt *et al.* have used a 6 DOF manipulator to build multi-resolution 3D printed parts with conformal layers [8, 12]. Shembekar *et al.* have explored the tool-path gener-

ation for performing 3D printing on non-planar substrates using 6 DOF manipulator [19]. Alsharhan *et al.* have improved the mechanical properties of the part using 6 DOF manipulators to 3D print it [20]. Zhao *et al.* have developed non-planar slicing techniques to build conformal 3D printed parts using manipulators [21]. Kraljić *et al.* have studied the trajectory planning problem to 3D print conformal layers [22]. Many other older works on robotic conformal 3D printing appear in these reports [23–25].

As research efforts in this area were largely focused on printing functional materials and devices, there has been a lack of quantitative investigation on the printing accuracy, for instance, the precise control of the gap between the tool tip and the target surface and geometric accuracy of printed patterns. Also, to the best of our knowledge, there have been no reports on using 6 DOF articulated manipulators for mesoscale conformal 3D printing on non-planar surfaces.

3 Experimental Setup

Figure 2 shows the experimental setup used in this study. The robotic manipulator used is 6 DOF Yaskawa Motoman GP8 manipulator. The Motoman GP8 is an articulated industrial manipulator with a payload of 8 kg, 727 mm reach, and rated repeatability of 0.02 mm. Its applications in the industry include handling, assembly, pick and place, and quality testing [26]. We select this manipulator due to its high repeatability and large workspace. Also, the 6 DOF of the manipulator offers desired flexibility to perform conformal printing. The Yaskawa manipulator is controlled using the YRC 1000 microcontroller.

There are three types of sensors used in the experimental setup. The first sensor is the Hexagon Absolute ROMER arm with an integrated laser scanner. It has a volumetric accuracy of $\pm$ 0.051 mm. It is used for workpiece registration described in Section 4.1. The second type of sensor is the RGB camera. Two cameras (FLIR) with Computar MLH-10X macro zoom lens (13 - 130 mm) are used. These two cameras are used for the Tool Center Point (TCP) estimation described in Section 4.2. The third type of sensor used in the experimental setup is the Laser Displacement Sensor (LDS; Optex CD33-30N-422) with a measurement range of 30 mm $\pm$ 4 mm and repeatability of 2 μm. This LDS is used for the gap compensation described in Section 4.3.

For the demonstration of conformal printing, a water-soluble gel ink material (Cellink Start) is deposited using a pneumatic fluid dispenser (Ultimus II, Nordson EFD) through a syringe with a ceramic tip (inner diameter: 50 μm). The syringe is mounted at 45° angle with respect to the LDS. Silicone elastomer (Dragon Skin, Smooth-On) is used for creating non-planar substrates through a molding process. The silicone elastomer substrates are treated with oxygen plasma before printing to enhance the wettability of the gel ink on the substrates. The approach using this experimental setup is described in Section 4.

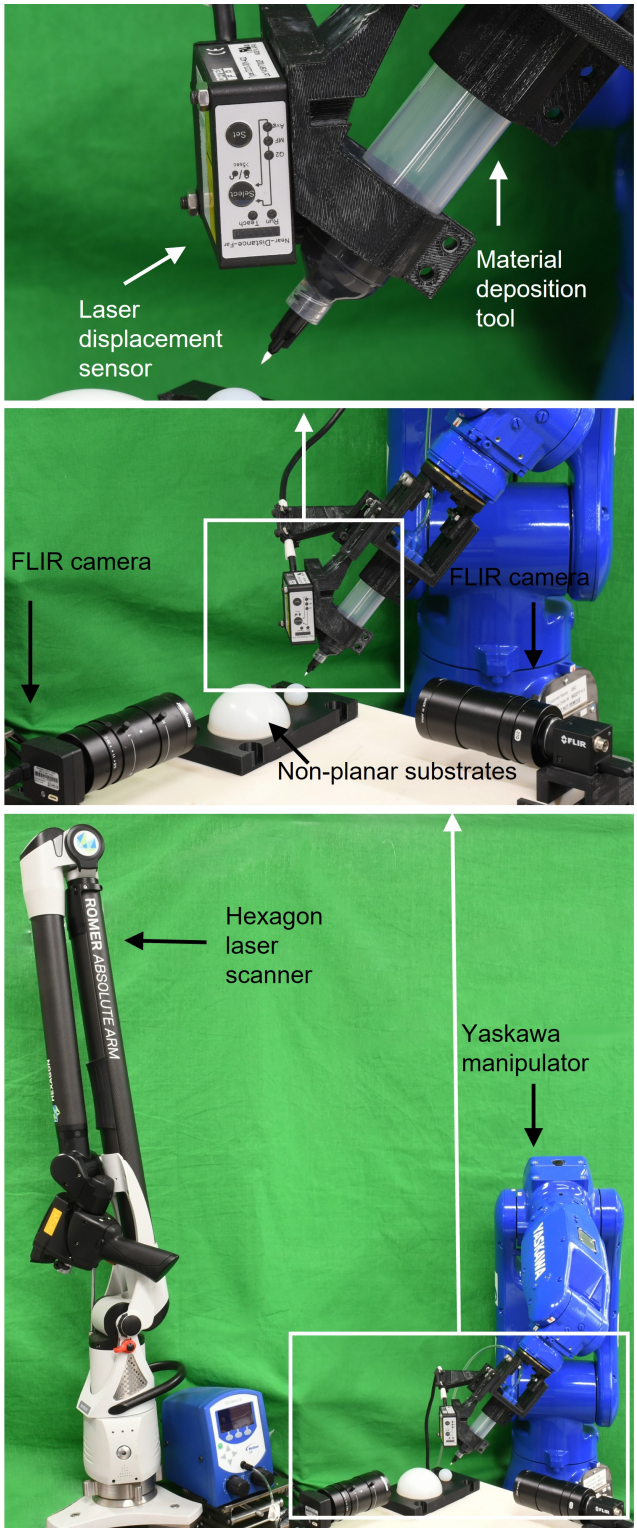

FIGURE 2: Experimental setup for mesoscale robotic conformal 3D printing.

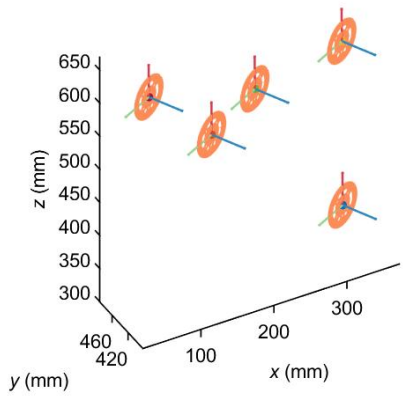

FIGURE 3: Scanned and filtered point clouds of the robot flanges for different robot configurations. Orange circle: flange; red line: x axis of the flange; green line: y axis of the flange; blue line: z axis of the flange.

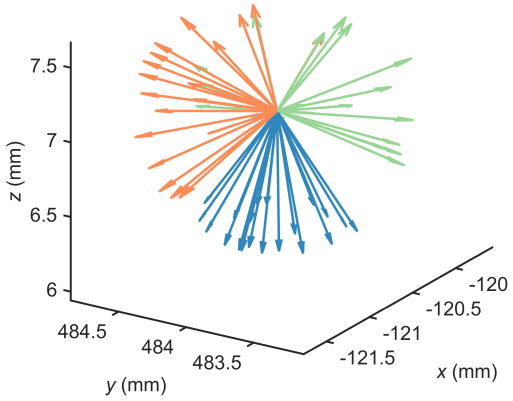

FIGURE 4: Illustration of the m orientations with which the manipulator tool tip can reach a target point in the view frames of both the cameras. Orange arrow: x axis of the tip; green arrow: y axis of the tip; blue arrow: z axis of the tip.

4 Approach

To realize conformal printing of mesoscale features using the manipulator, we first perform the workpiece registration in Section 4.1 to obtain the relative position of the robot base frame and the substrate. Then the accurate TCP estimation in Section 4.2 is utilized to identify the tool tip's position relative to the robot flange frame, followed by compensating the gap between the tool tip and the surface of the pre-existing non-planar substrate in Section 4.3 to reduce gap errors. The robot base frame $\{B\}$ is located on the base link of the manipulator, which is mounted to the ground. The robot flange frame $\{F\}$ is located on the last

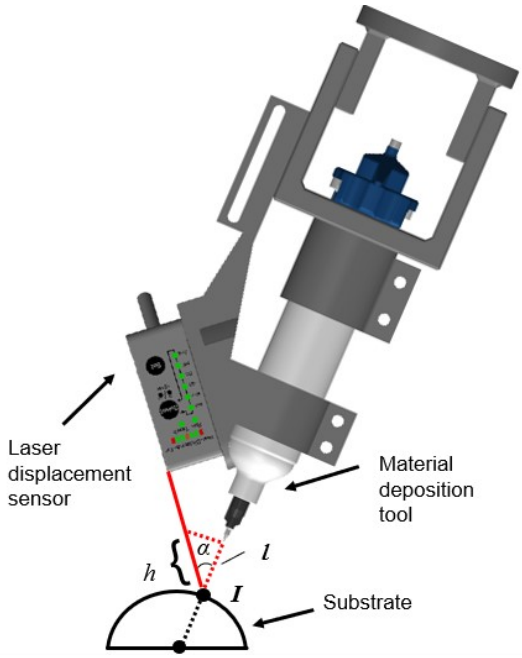

FIGURE 5: Schematic illustration of the placement of the laser displacement sensor for gap compensation. Red solid line: laser beam.

link of the manipulator. The tool is mounted to the flange. The tool tip's frame $\{t\}$ is located on the tip of the tool.

4.1 Workpiece Registration

Workpiece registration is necessary to localize the substrate in the robot base frame. We use the data generated using the Hexagon laser scanner and the following steps to realize it.

1. In the first step, we drive the manipulator to n different configurations and record the joint angle vectors of the manipulator $\vec{\theta}$ for each configuration. Using the Equation 1, the transformation matrix from the robot base frame to the flange frame $\{F\}$ represented as T_F^B is calculated for each configuration.

$$T_F^B = \mathrm{FK}(\vec{\theta}) \tag{1}$$

   Here $\mathrm{FK}(\cdot)$ represents the Forward Kinematics function to obtain the transformation matrix from the robot base frame to the robot flange frame using the joint angles [27].
2. In the next step, the Hexagon laser scanner is used to scan the robot flange for the n configurations. The scanned robot flanges after filtering the noise by clustering are shown in Figure 3. Using the flange point clouds we can get the transformation matrix from the laser scanner base frame $\{L\}$ to the robot flange frame, i.e. T_F^L. This is realized by assigning the transformation location as the center of each flange point cloud and the transformation z axis as the normal to

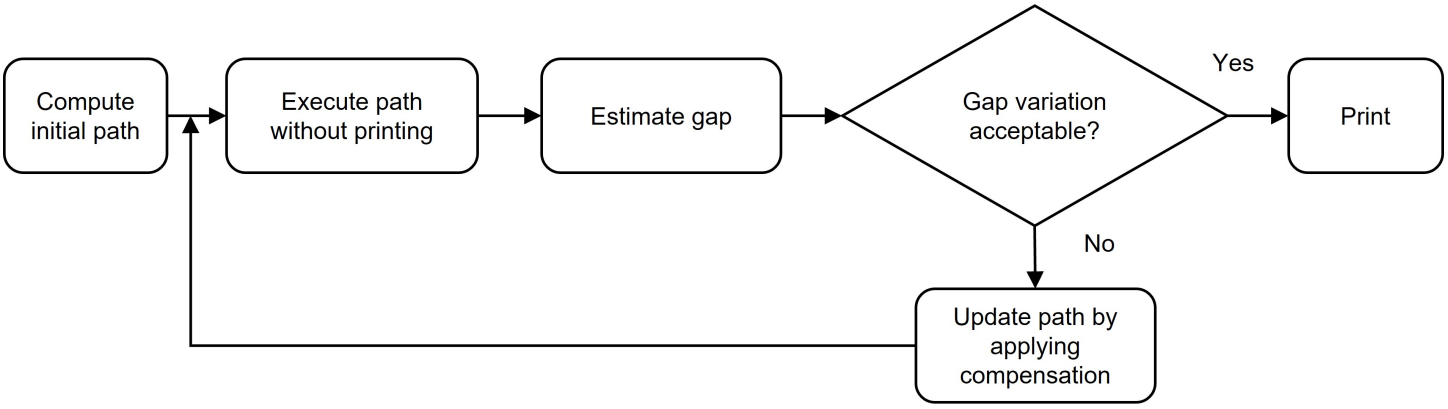

FIGURE 6: Flowchart indicating the steps in the gap compensation process.

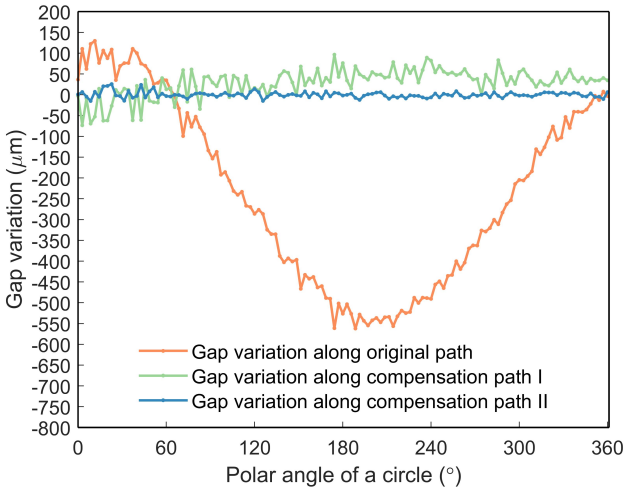

FIGURE 7: Gap variations along paths for printing a circle on a hemispherical surface.

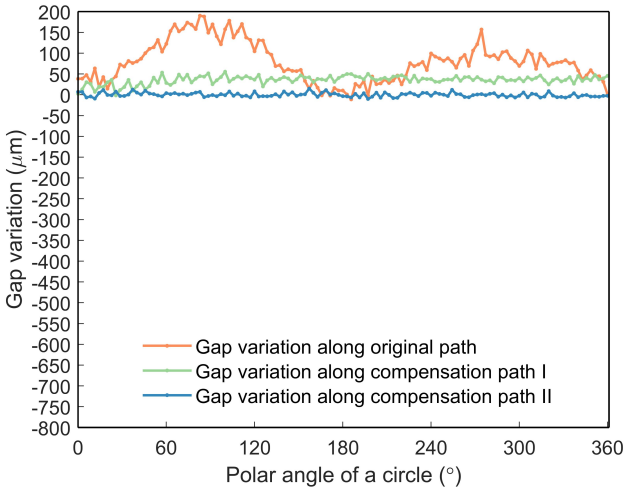

FIGURE 8: Gap variations along paths for printing a circle on a cylindrical surface.

the plane containing the point cloud. The x and y axes of the transformation matrix are placed perpendicular to the z axis.

3. In the final step, the transformation matrix T_B^L from the laser scanner base frame to the robot base frame is calculated numerically by applying the least square method using the Equations 2-3.

$$T_B^L = T_F^L (T_F^B)^{-1} \tag{2}$$

$$\vec{0} = \sum_{i=1}^{n-1} \sum_{j=i+1}^{n} ((\vec{v}_{T_B^L})_i - (\vec{v}_{T_B^L})_j) \tag{3}$$

Here $\vec{v} =< x, y, z, f \times \vec{q} >$ is a vector encoding the transformation matrix T_B^L, $\vec{q}$ is the vector containing the quaternions of the transformation matrix, and $< x, y, z >$ are the translation vector of of the transformation matrix. f is a weight multiplication factor.

The position of the substrate in the laser scanner base frame is known by scanning the substrate. Thus, by using the relative positions of the robot base frame and the substrate in the laser scanner base frame we can register the workpiece, i.e, the substrate in the robot base frame.

4.2 Accurate TCP Estimation

The tip of the conical tool is set as the TCP which needs to be estimated accurately. To determine the TCP, we estimate the tool tip location in the robot flange frame as the location of the robot flange frame with respect to the robot base frame can be obtained by the Equation 1. This estimation is enabled using two cameras (see Figure 2). In the setup, the cameras are approximately placed parallel to the horizontal plane, and perpendicular to each other. The tool tip is simultaneously monitored in these two cam-

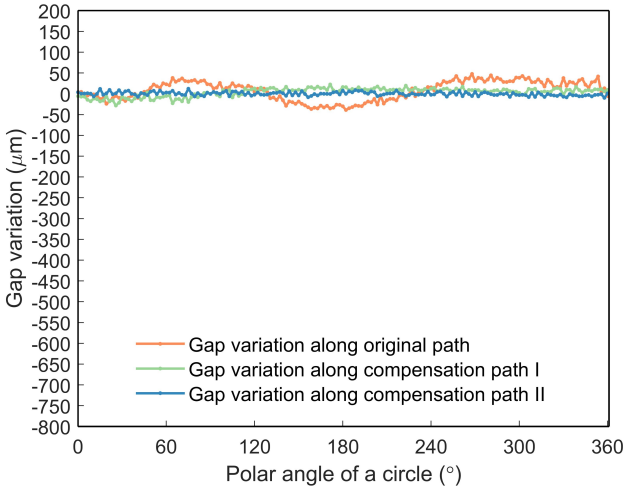

FIGURE 9: Gap variations along different paths for printing a circle on a planar surface.

eras. We estimate the TCP using the following steps.

1. In the first step, we select a target point which is visible in both cameras. Then, m different poses for the tool tip reaching the target point (see Figure 4) are calculated using an initial, approximate value of the TCP.
2. In the second step, the manipulator is driven to the m poses. The tool tip is detected by processing the images captured by the cameras. Due to the approximation of the initial TCP value, the TCP has different camera pixel values for all the m poses. The pixel error is calculated and the manipulator is servo-controlled in real time to match the tool tip pixel for the m poses. The joint values of the manipulator $\vec{\theta}$, for all the matched pixel configurations are recorded. By substituting $\vec{\theta}$ into the Equation 1, we can obtain T_F^B.
3. In the final step, the least square method, is used to accurately estimate the location of the TCP in the robot flange frame by using the Equations 4-6.

$$T_t^F = \begin{bmatrix} 1 & 0 & 0 & x_t \\ 0 & 1 & 0 & y_t \\ 0 & 0 & 1 & z_t \\ 0 & 0 & 0 & 1 \end{bmatrix} \tag{4}$$

$$T_t^B = T_F^B T_t^F \tag{5}$$

$$\vec{0} = \sum_{i=1}^{m-1} \sum_{j=i+1}^{m} ((\vec{v}_{T_t^B})_i - (\vec{v}_{T_t^B})_j) \tag{6}$$

Here T_t^F denotes the transformation matrix from the robot flange frame to the tool tip's frame. We assign the tool tip's frame to have the same orientation as the robot flange frame. Therefore, only the translation in the transformation matrix $< x_t, y_t, z_t >$ needs to be recognized here. T_t^B denotes the transformation matrix from the robot base frame to the tool tip's frame.

4.3 Gap Compensation

After the workpiece registration and the accurate TCP estimation, there are still gap errors existing between the tool tip and the surface of the substrate when we try to drive the manipulator to deposit materials on the non-planar substrate. The gap errors originate from multiple sources, including the laser scanner's accuracy, the operating errors, the image processing errors, the calculation errors, and DH parameters' errors. To avoid the tool tip bumping into the substrate surface and to ensure the continuity of ink deposited, a gap compensation is needed.

In this section, we present a means for the gap compensation by using the LDS installed near the tool tip. In Figure 5, Point I is the intersection of the LSD's laser beam and the extension line of the tool tip's axis. The distance between the point I and the end of the tool tip is l. The value of l is the gap that needs to be maintained, which can be calculated by the Equation 7.

$$l = h\cos(\alpha) \tag{7}$$

Here α is the installation angle between the syringe and the LDS. h can be measured by the LDS.

To compensate for the gap before printing, we utilize the LDS to scan the substrate surface by executing the printing path without depositing the ink material. The gap between the tool tip and the substrate surface is calculated by the Equation 7 and the compensation is calculated. The compensated path generated by independently varying the tool tip's position along the tool tip's axis over the path is executed again without depositing the ink. If the point I is maintained on the substrate surface along the compensated path, (i.e., the distances between the tool tip and the substrate surface are constant as l_0 which can be measured by using one of the two cameras in Figure 2), printing can be performed by moving the tool tip around $l_0 - 40$ μm down along the axis of the tool tip along the compensated path. Otherwise, the compensation process is repeated (see Figure 6).

Figure 7 - Figure 9 show that after performing compensation twice, the gap's variations are decreased from 692 μm to within 40.7 μm, from 201 μm to within 25 μm, and from 87 μm to within 22 μm, respectively, when tracing circles. We observed similar trends in other geometries.

5 Experimental Results

Three sets of experiments are performed in this paper: testing the influence of the gap between the tool tip and the substrate;

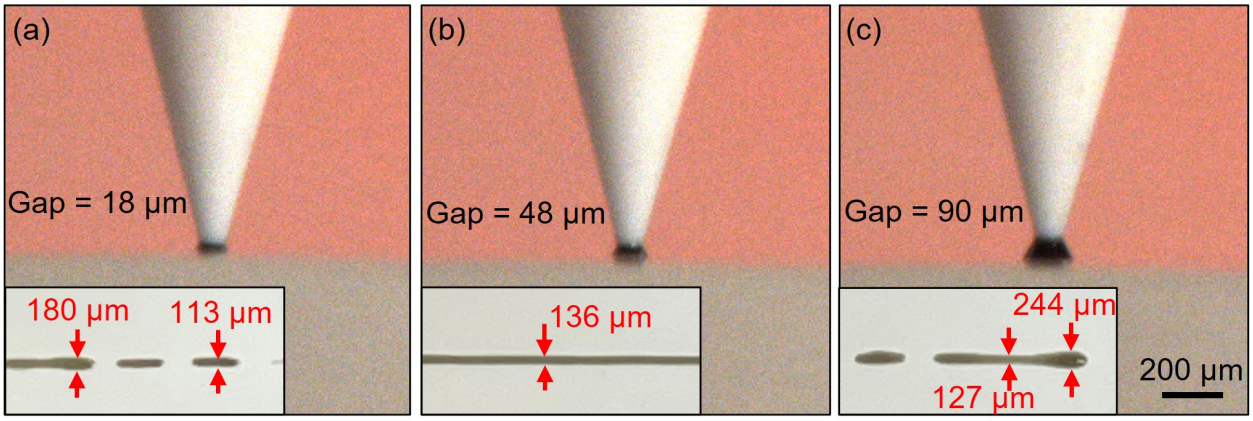

FIGURE 10: Side-view images of different gaps between the tool tip and a flat surface and the corresponding printed lines (insets). The gaps in (a), (b) and (c) are 18 μm, 48 μm, and 90 μm, respectively.

testing the efficacy of the proposed approach; and demonstrating the advantages of using the 6 DOF robotic manipulator to deposit materials on curved surfaces by changing the tool orientation.

We first test the influence of the gap (defined as the distance between the middle point of the tool tip and the substrate) on the printing quality. This gap is found to be a critical parameter for successful printing. In this experiment, the tool is parallel to a flat substrate's normal direction. In this configuration, a relatively small gap (e.g. 18 μm) can cause discontinuous extrusion of ink (Figure 10 a), while a relatively large gap (e.g. 90 μm) leads to the generation of ink droplets (Figure 10 c). The appropriate gap is experimentally found to be approximately between 25 $\pm$ 5 μm to 75 $\pm$ 5 μm for successful printing with line widths to be within the 100 μm to 160 μm range (Figure 10 b). This sets the requirements for the gap variation given the repeatability errors of the manipulator.

To test the efficacy of the proposed approach, we print three different types of patterns (i.e. circle, spiral and serpentine lines) on planar, cylindrical, and hemispherical substrates with the gap in the appropriate range determined from the tests above.

To print these patterns in Figure 11-13, we first ortho project a circle, a spiral, or a serpentine pattern on the horizontal plane to the non-planar surfaces (or a planar surface) to obtain the new print pattern. Then, the printing path of the manipulator is calculated based on the newly obtained pattern, the registration of the workpiece and the result of the TCP estimation, followed by the gap compensation. Finally, the gap between the tool tip and the target surfaces is within the appropriate range.

As shown in Figure 11 and Figure 12, gap compensation is necessary for successful printing of the complete patterns. After the 1st gap compensation, the printing quality is improved. Finally, after the 2nd compensation, we are able to successfully print the complete patterns on the cylindrical (30 mm radius) and hemispherical (30 mm radius) surfaces.

The line widths of the circular, spiral and serpentine patterns printed on planar surfaces are measured using an optical microscope (Figure 13). Except for the beginning and end points (likely due to partial dewetting of ink on the substrate), the line widths typically range from 100 μm to 160 μm.

While a vertical tool orientation can support printing on curved surfaces with a relatively large radius of curvature as demonstrated above, conformal printing on highly curved surfaces requires changing tool orientation with respect to the target surface. Here, we demonstrate the necessity and capability of changing the tool orientation for printing on surfaces with a radius of curvature smaller than 1 cm (a video of the demonstration appears in [28]). The print patterns are obtained by ortho projecting circles on tangent planes to the spherical surface. A series of circles are ortho projected and printed in Figure 14 and Figure 15 on a spherical surface with 9 mm in radius. When the axis of the tool tip is kept vertical during the printing process, the printed pattern becomes discontinuous starting approximately from the point with the normal that is 17° from the vertical axis (Figure 14). When the axis of the tool tip is adjusted to align with the normals of points on the spherical surface, a continuous circular pattern can be printed on the spherical surface (Figure 15). This comparison shows that adjusting the tool orientation with respect to the target surface is critical in enabling continuous conformal printing on highly curved surfaces. We reproject the printed circles and ideal circles on a perfect sphere to the horizontal plane, and calculate and compare their aspect ratios. The mean error of 7 printed patterns is 3.0 % with the maximum error of 6.8 %. The sources of error include the positioning error of the manipulator, the sensitivity of the laser scanner and the LDS to the substrate, the substrate's imperfect spherical shape, the error in image processing, the operation error of the laser scanner, the assemble error of the tool tip and the LDS, and the calculation error of the method proposed in this paper.

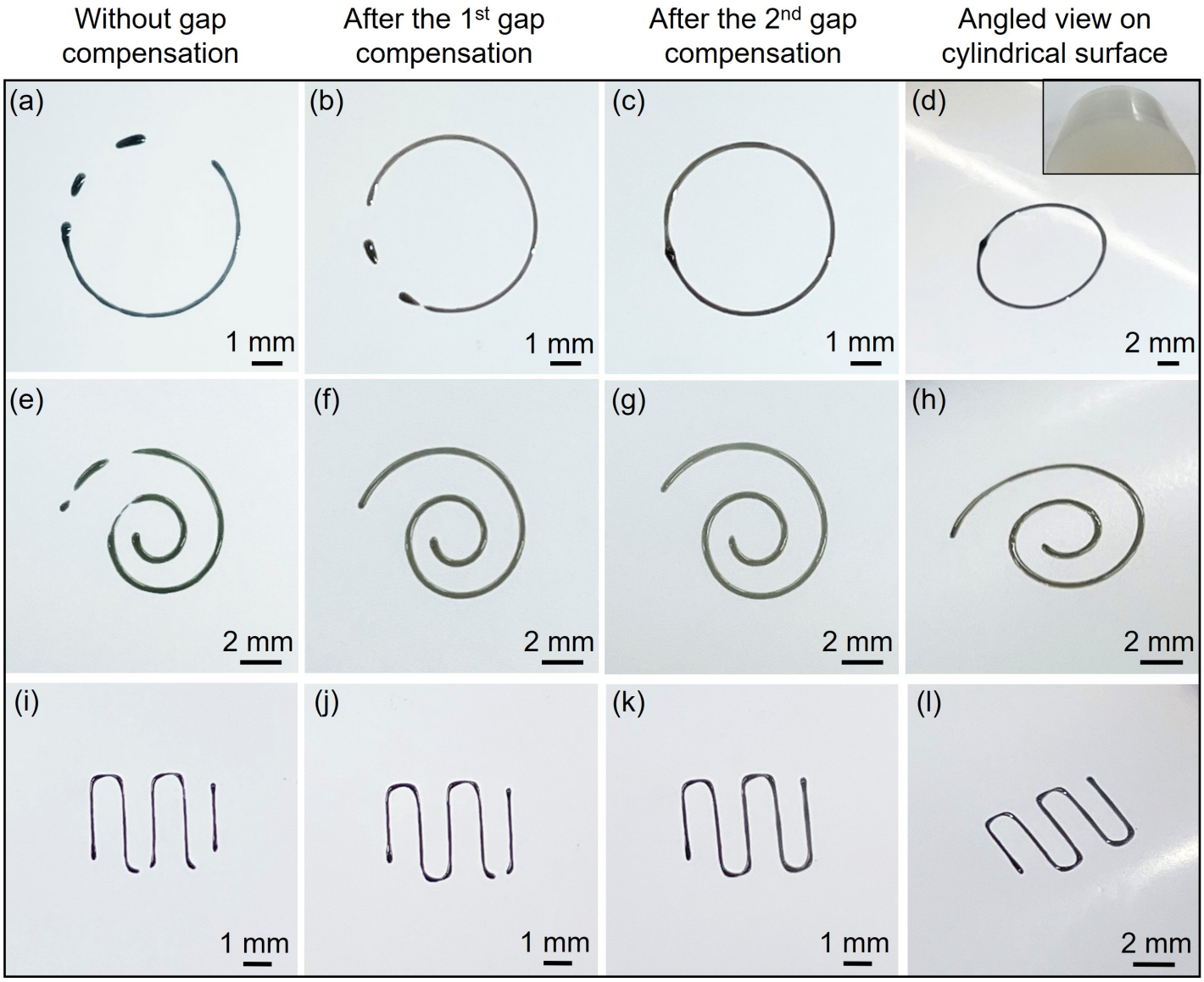

FIGURE 11: Optical images of printed patterns on a cylindrical surface. (a)-(d): circle; (e)-(h): spiral; (i)-(l): serpentine lines. (a)-(c), (e)-(g) and (i)-(k) are top-down view and (d)(h)(i) are side view of the printed patterns. (a)(e)(i) are prints without gap compensation; (b)(f)(j) are prints after the 1st gap compensation; (c)(g)(k) are prints after the 2nd gap compensation. Inset in (d) is an optical image of the cylindrical surface (3 cm in radius).

6 Characterizing the Effect of Inaccuracy in Robot Kinematic Model on Gap Variation

The manipulator executed the computed path during the first trial without any compensation. We now analyze variability in the gap. We use circles as the reference geometry during this analysis. When the manipulator tries to trace a circle in the space, the actual circle traced by the manipulator might be shifted in location and orientation due to errors in the estimated robot kinematic model. We use the Denavit–Hartenberg (DH) parameters to model robot kinematics. Figure 16 shows an example of such a shift. The shift based on the original circle center is $\Delta x = -6.4$ mm, $\Delta y = 2.3$ mm, $\Delta z = 4.4$ mm and orientation error of 2.1°. If the traced circle is shifted with its intended location, then the gap measured by the laser in the manipulator will exhibit variability. We have simulated shifts in the circle location and orientation and estimated the gap between the tool tip and the hemispherical substrate. Figure 17 shows the result based on the circle center error corresponding to $\Delta x = 3$ mm, $\Delta y = 1.5$ mm and orientation error of 0.5°. This result matches our experimental observations.

Tracing a circle on a cylinder requires the circle to be dis-

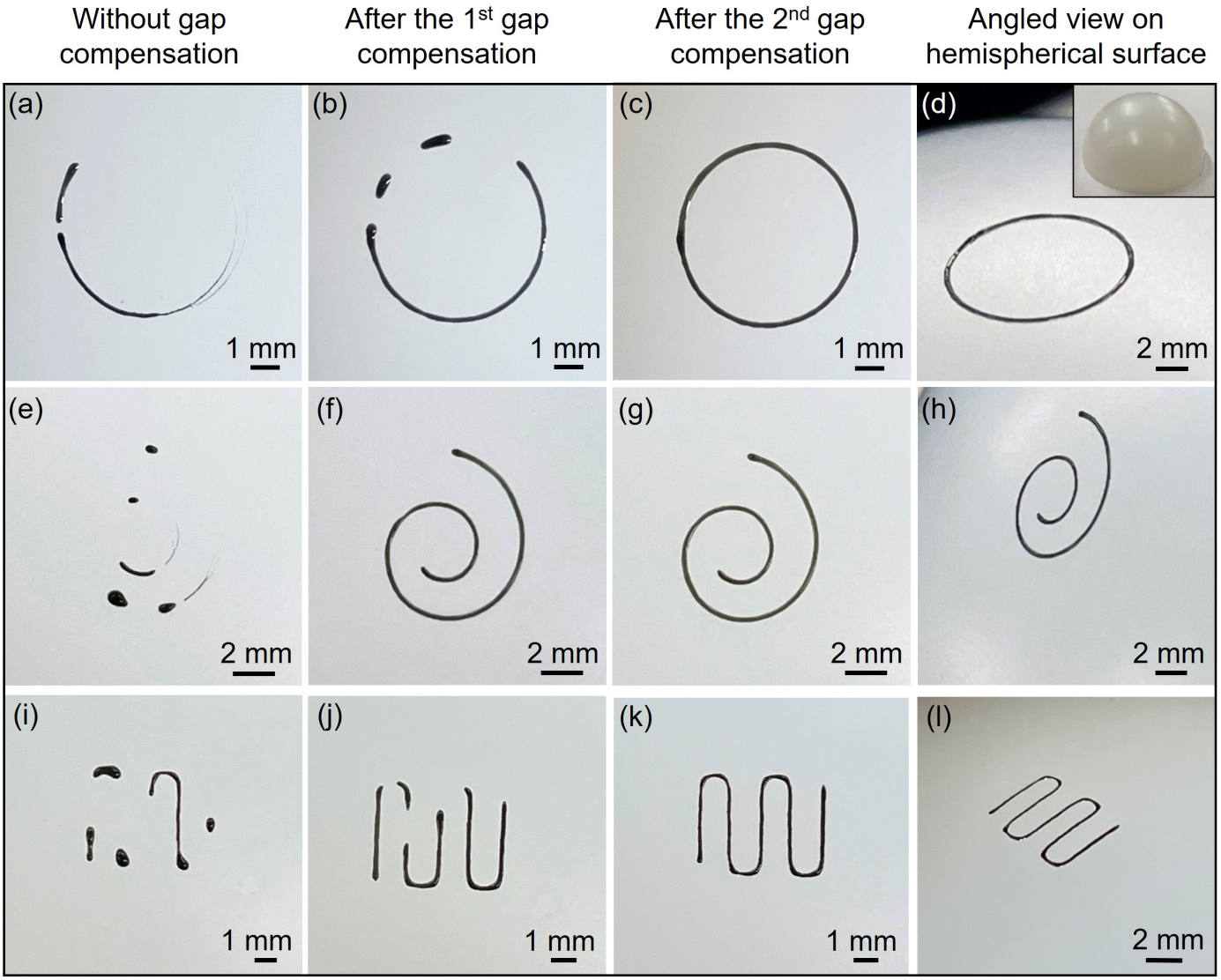

FIGURE 12: Optical images of printed patterns on a hemispherical surface. (a)-(d): circle; (e)-(h): spiral; (i)-(l): serpentine lines. (a)-(c), (e)-(g) and (i)-(k) are top-down view and (d)(h)(i) are side view of the printed patterns. (a)(e)(i) are prints without gap compensation; (b)(f)(j) are prints after the 1st gap compensation; (c)(g)(k) are prints after the 2nd gap compensation. Inset in (d) is an optical image of the hemispherical surface (3 cm in radius).

torted and wrapped around the cylinder (See Figure 18). This means that the geometry being traced exhibits significant out-of-plane motion. Errors in DH parameter estimations now not only introduce a shift in the circle center and its location but also cause errors in the out-of-plane motion. This means that the circle does not deform to perfectly wrap around the cylinder, therefore we observe variations in the gap. We have simulated the shift in the circle location and orientation and estimated the gap based between the tool tip and the cylindrical substrate. Figure 19 shows the result based on the circle center error corresponding to $\Delta x = 0$ mm, $\Delta y = 0.1$ mm, orientation error of 0.5°, and Z-discrepancy of 76 μm. This result matches our experimental observations. The gap variation now exhibits a double peak.

When we print a circle on a nominally planar surface, the gap variations are expected to be significantly smaller for the same level of errors in DH parameters. Our experimental data shown in Figure 9 confirms this. Errors in the center location and orientation of the non-ideal planar surface result in variations in the gap. The double-peak variation shown in Figure 9 can be caused by small curvature of the nominally planar surface. The height variation is of the planar surface is measured to be approximately 40 μm along a line in the middle of the surface. This height variation leads to gap variations without compensation.

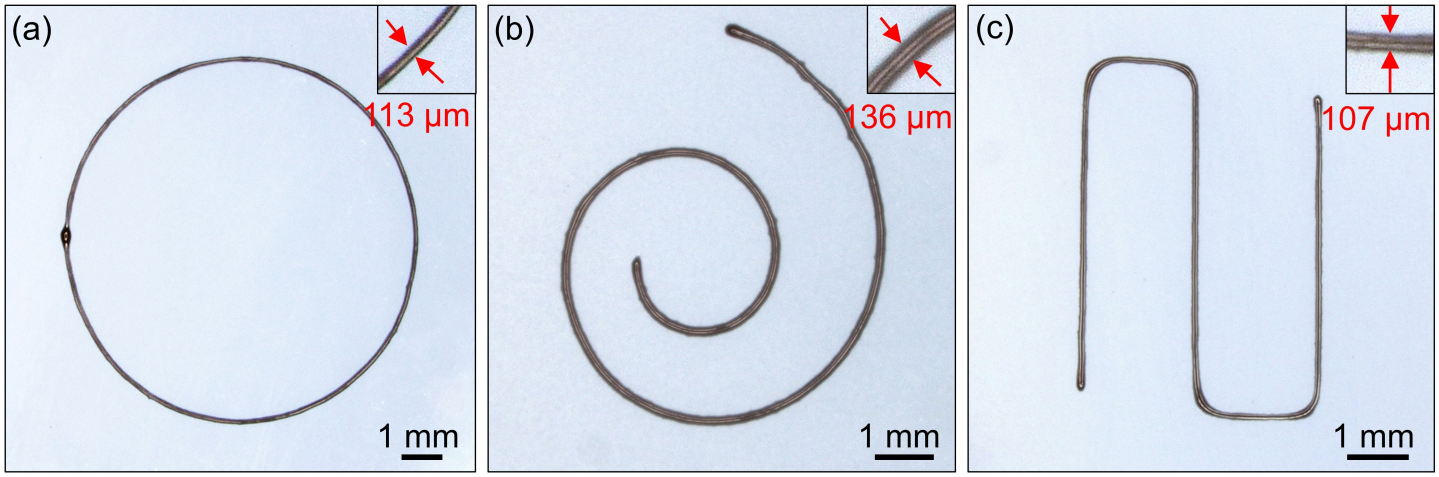

FIGURE 13: Optical images of printed patterns after the 2nd gap compensation on a flat surface. (a): circle; (b): spiral; (c): serpentine lines. Insets show the measured line widths.

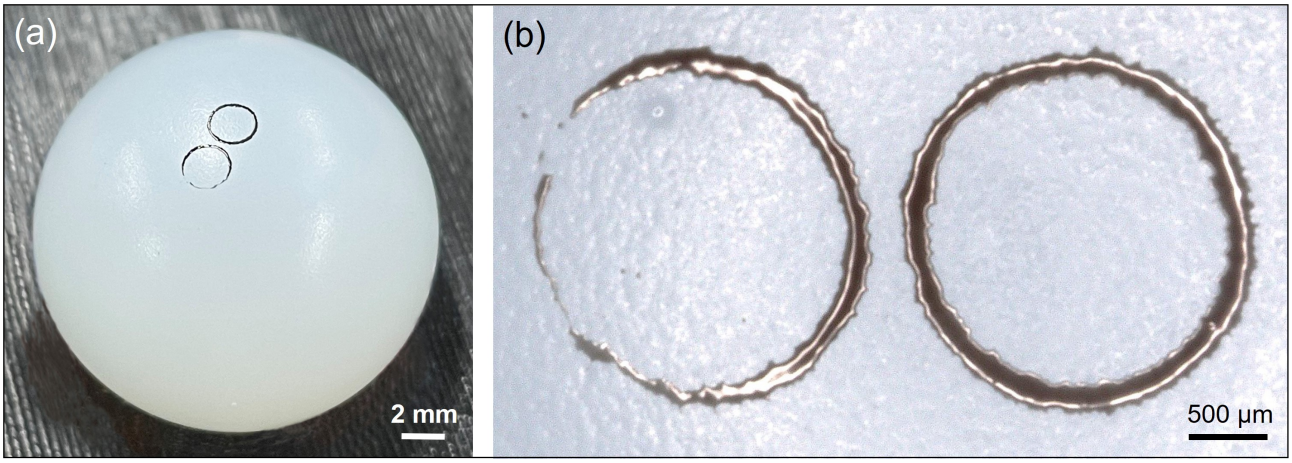

FIGURE 14: Optical images of printed circles (1 mm in radius) after the 2nd gap compensation on a small spherical surface (9 mm in radius) by maintaining a vertical tool tip orientation. (a) is side view and (b) is top-down view of the printed circles.

We used the measured gap variation from the first run to modify the manipulator path to reduce the gap variations in subsequent runs. We did not use gap variability to improve the robot kinematic model in the current work. Future work may include using gap variability observed on the first run to update the robot kinematic model and reduce the number of compensation steps required to maintain the appropriote gap during conformal printing.

7 Conclusions

We have demonstrated that industrial robotic manipulators can be used to perform conformal deposition with mesoscale features on non-planar surfaces. Here is a summary of the main results presented in this paper:

1. Using a 6 DOF manipulator with multiple sensors, including the LDS and cameras, we realized printing different patterns with line widths within 100-160 μm;
2. Leveraging the high repeatability of the manipulator and the LDS, we demonstrated that the gap variation can be reduced to approximately 40 μm by using the proposed compensation scheme;
3. By adjusting the tool tip's axis to align with the normal direction of the target surface along the printing path, the 6 DOF manipulator exhibits unique advantages in conformal printing on highly curved surfaces as compared to printing with constant tool orientation;
4. Through simulations, we investigated the sources of gap variations. This can be used in the future to improve the kinematic model of the robot.

The approach presented in this study provides a means of

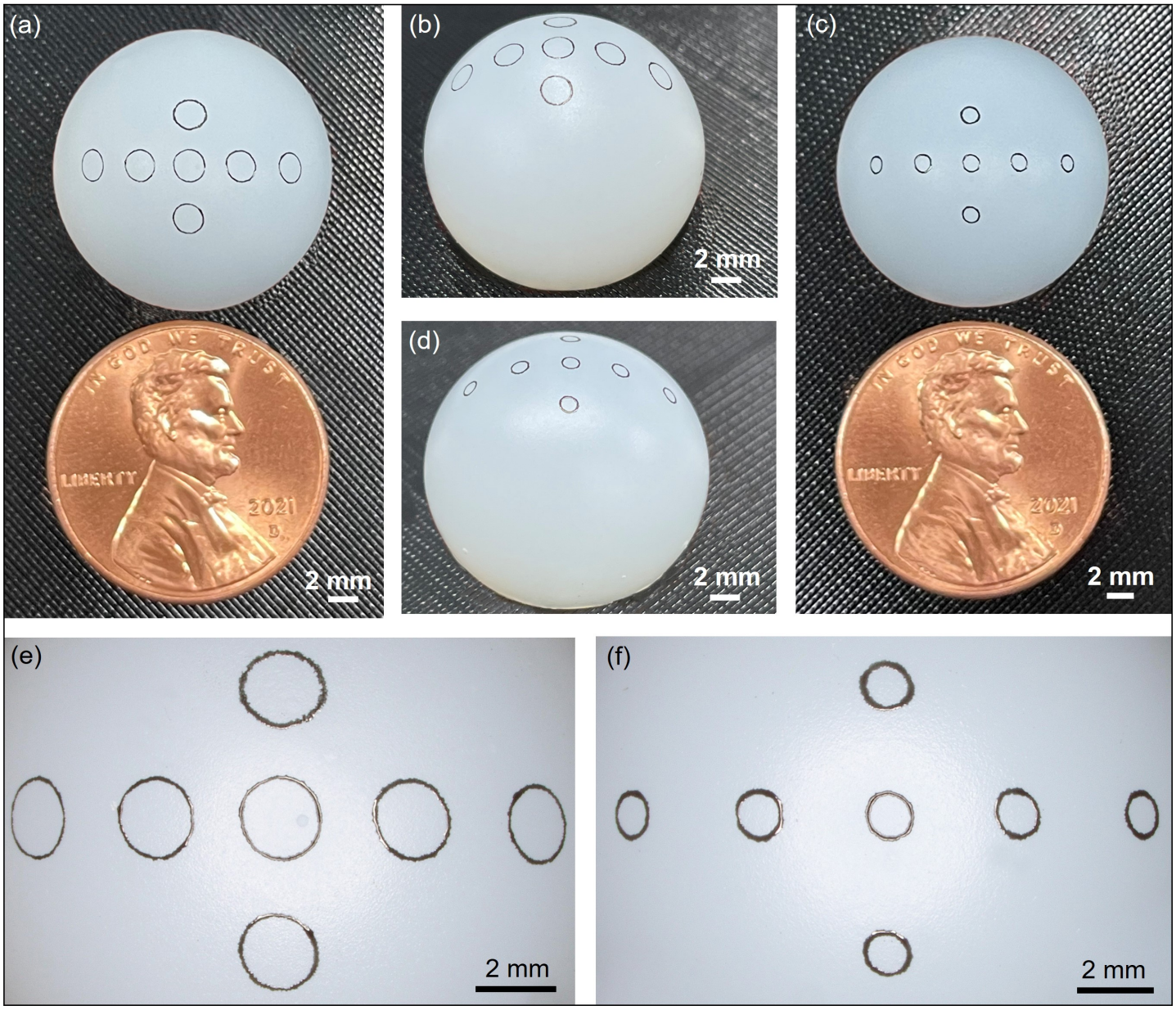

FIGURE 15: Optical images of different sizes of printed circles after the 2nd gap compensation on a small spherical surface (9 mm in radius) by adjusting the axis of the tool tip normal to each point on the substrate surface. (a)(b)(e): circles with 1 mm radius; (c)(d)(f): circles with 0.6 mm radius; (a)(c)(e) and (f) are top-down view and (b)(d) are side view of the printed circles.

achieving conformal deposition with mesoscale features, which may find applications in 3D functional electronics, optoelectronics, sensors, and microfluidic devices on non-planar surfaces or prefabricated components without planar approximation. Future work includes further improvement on the manipulator's positioning accuracy for high-resolution conformal printing. The adjustment of tool orientation in 3D space with respect to target surfaces leveraging the 6 DOF robotic manipulators can significantly increase the capability of printing on geometrically complex 3D surfaces such as concave surfaces with a small radius of curvature and irregular surfaces. The use of multiple print heads with automatic switching may enable multi-material conformal printing for functional devices on target surfaces.

Acknowledgement: This work is supported in part by National Science Foundation Grant #1925084. Opinions expressed are those of the authors and do not necessarily reflect the opinions of the sponsors.

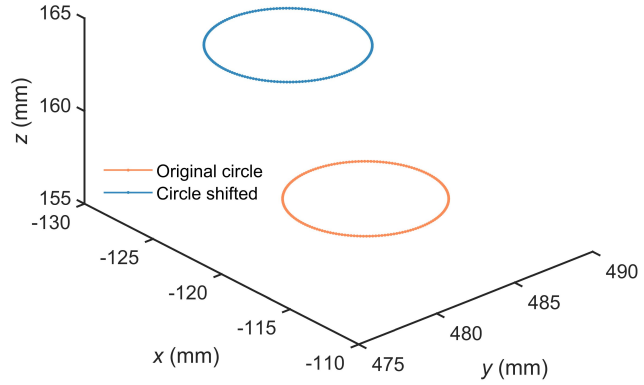

FIGURE 16: Simulation of the circle shifted by inducing offsets of 24 DH parameters (0.5 mm offset for the length and 0.5° offset for the angle).

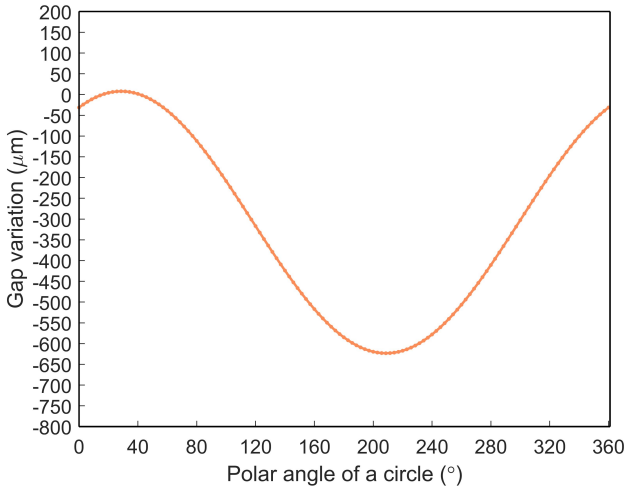

FIGURE 17: Simulation of gap variations along the original path for printing a circle on a hemispherical surface.

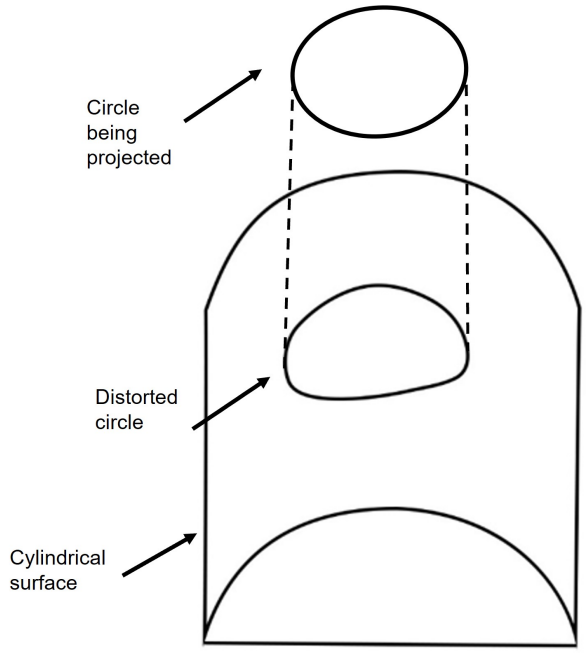

FIGURE 18: Schematic illustration of tracing a circle on a cylindrical surface.

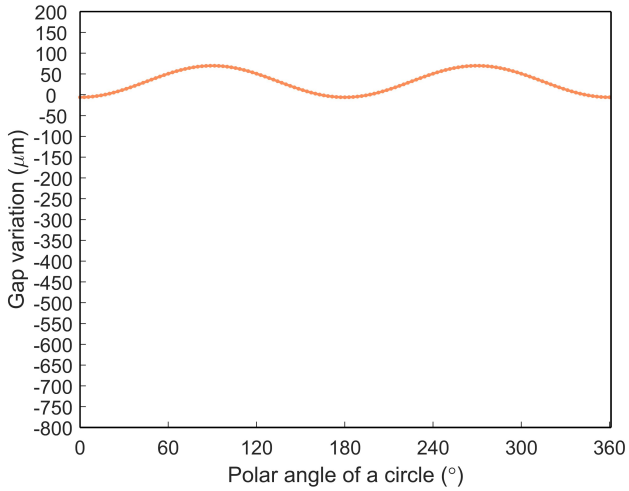

FIGURE 19: Simulation of gap variations along the original path for printing a circle on a cylindrical surface.

References

[1] Gibson, I., Rosen, D. W., and Stucker, B., 2010. *Additive manufacturing technologies: rapid prototyping to direct digital manufacturing*. Springer.

[2] Huang, Y., Wu, H., Xiao, L., Duan, Y., Zhu, H., Bian, J., Ye, D., and Yin, Z., 2019. "Assembly and applications of 3d conformal electronics on curvilinear surfaces". *Mater. Horiz.,* ***6***, pp. 642–683.

[3] Zhu, Z., Ng, D. W. H., Park, H. S., and McAlpine, M. C., 2021. "3d-printed multifunctional materials enabled by artificial-intelligence-assisted fabrication technologies". *Nature Reviews Materials,* ***6***(1), pp. 27–47.

[4] Kaur, M., Kim, T.-H., and Kim, W. S., 2021. "New frontiers in 3d structural sensing robots". *Advanced Materials,* ***33***(19), p. 2002534.

[5] Adams, J. J., Duoss, E. B., Malkowski, T. F., Motala, M. J., Ahn, B. Y., Nuzzo, R. G., Bernhard, J. T., and Lewis, J. A.,

2011. “Conformal printing of electrically small antennas on three-dimensional surfaces”. *Advanced Materials,* ***23***(11), pp. 1335–1340.

[6] Zhu, Z., Guo, S.-Z., Hirdler, T., Eide, C., Fan, X., Tolar, J., and McAlpine, M. C., 2018. “3d printed functional and biological materials on moving freeform surfaces”. *Advanced Materials,* ***30***(23), p. 1707495.

[7] Su, R., Wen, J., Su, Q., Wiederoder, M. S., Koester, S. J., Uzarski, J. R., and McAlpine, M. C., 2020. “3d printed self-supporting elastomeric structures for multifunctional microfluidics”. *Science Advances,* ***6***(41), p. eabc9846.

[8] Bhatt, P. M., Kabir, A. M., Malhan, R. K., Shah, B. C., Shembekar, A. V., Yoon, Y. J., and Gupta, S. K., 2019. “A robotic cell for multi-resolution additive manufacturing”. In IEEE International Conference on Robotics and Automation.

[9] Yoon, Y. J., Shembekar, A. V., Almeida, O. G., and Gupta, S. K., 2020. “A robotic cell for embedding prefabricated components in extrusion-based additive manufacturing”. In ASME Manufacturing Science and Engineering Conference.

[10] Bhatt, P. M., Gong, C., Kabir, A. M., Malhan, R. K., Shah, B. C., and Gupta, S. K., 2020. “Incorporating tool contact considerations in tool-path planning for robotic operations”. In ASME Manufacturing Science and Engineering Conference, Vol. 84256, p. V001T05A018.

[11] Bhatt, P. M., Kabir, A. M., Malhan, R. K., Shembekar, A. V., Shah, B. C., and Gupta, S. K., 2019. “Concurrent design of tool-paths and impedance controllers for performing area coverage operations in manufacturing applications under uncertainty”. In IEEE International Conference on Automation Science and Engineering.

[12] Bhatt, P. M., Kulkarni, A., Malhan, R. K., Shah, B. C., Yoon, Y. J., and Gupta, S. K., 2021. “Automated planning for robotic multi-resolution additive manufacturing”. *Journal of Computing and Information Science in Engineering,* ***22***(2), p. 021006.

[13] Bhatt, P. M., Malhan, R. K., Rajendran, P., Shembekar, A. V., and Gupta, S. K., 2021. “Trajectory-dependent compensation scheme to reduce manipulator execution errors for manufacturing applications”. In ASME Manufacturing Science and Engineering Conference.

[14] Bhatt, P. M., Rajendran, P., McKay, K., and Gupta, S. K., 2019. “Context-dependent compensation scheme to reduce trajectory execution errors for industrial manipulators”. In IEEE International Conference on Robotics and Automation, pp. 5578–5584.

[15] Cohen, D. L., Lipton, J. I., Bonassar, L. J., and Lipson, H., 2010. “Additive manufacturing for in situ repair of osteochondral defects”. *Biofabrication,* ***2***(3), sep, p. 035004.

[16] Park, S. H., Su, R., Jeong, J., Guo, S.-Z., Qiu, K., Joung, D., Meng, F., and McAlpine, M. C., 2018. “3d printed polymer photodetectors”. *Advanced Materials,* ***30***(40), p. 1803980.

[17] Kim, T., Bao, C., Hausmann, M., Siqueira, G., Zimmermann, T., and Kim, W. S., 2019. “3d printed disposable wireless ion sensors with biocompatible cellulose composites”. *Advanced Electronic Materials,* ***5***(2), p. 1800778.

[18] Bhatt, P. M., Malhan, R. K., Shembeka, A. V., Yoon, Y. J., and Gupta, S. K., 2020. “Expanding capabilities of additive manufacturing through use of robotics technologies: A survey”. *Additive Manufacturing,* ***31***, January, p. 100933.

[19] Shembekar, A. V., Yoon, Y. J., Kanyuck, A., and Gupta, S. K., 2019. “Generating robot trajectories for conformal 3d printing using non-planar layers”. *ASME Journal of Computing and Information Science in Engineering,* ***19***(3), September, p. 031011.

[20] Alsharhan, A., Centea, T., and Gupta, S. K., 2017. “Enhancing the mechanical properties of thin-walled structures using non-planar extrusion-based additive manufacturing”. In ASME Manufacturing Science and Engineering Conference.

[21] Zhao, G., Ma, G., Feng, J., and Xiao, W., 2018. “Nonplanar slicing and path generation methods for robotic additive manufacturing”. *The International Journal of Advanced Manufacturing Technology,* ***96***(9-12), pp. 3149–3159.

[22] Kraljić, D., and Kamnik, R., 2018. “Trajectory planning for additive manufacturing with a 6-dof industrial robot”. In International Conference on Robotics in Alpe-Adria Danube Region, Springer, pp. 456–465.

[23] Jin, Y., Du, J., He, Y., and Fu, G., 2017. “Modeling and process planning for curved layer fused deposition”. *The International Journal of Advanced Manufacturing Technology,* ***91***(1-4), pp. 273–285.

[24] Lim, S., Buswell, R. A., Valentine, P. J., Piker, D., Austin, S. A., and De Kestelier, X., 2016. “Modelling curved-layered printing paths for fabricating large-scale construction components”. *Additive Manufacturing,* ***12***, pp. 216–230.

[25] Kim, C., Espalin, D., Cuaron, A., Perez, M. A., Lee, M., MacDonald, E., and Wicker, R. B., 2015. “Cooperative tool path planning for wire embedding on additively manufactured curved surfaces using robot kinematics”. *Journal of Mechanisms and Robotics,* ***7***(2), p. 021003.

[26] Cai, Y., Han, Z., Cranney, T., Zhao, H., and Gupta, S. K., 2021. “Automated robotic assembly of 3d mesostructure via guided mechanical buckling”. In 2021 IEEE 17th International Conference on Automation Science and Engineering (CASE), IEEE, pp. 2098–2104.

[27] Spong, M. W., Hutchinson, S., Vidyasagar, M., et al., 2006. *Robot modeling and control*.

[28] Cai Y., Bhatt P. M., Zhao H. and Gupta S. K., 2022. “Using an articulated industrial robot to perform conformal deposition with mesoscale features”. https://www.youtube.com/watch?v=guZhWPAojbI.